Ground-state configurations and theoretical soft-x-ray emission of highly charged actinide ions

J. Sheil,* D. Kilbane, and G. O'Sullivan
School of Physics, University College Dublin, Belfield, Dublin 4, Ireland

L. Liu
School of Physics, University College Dublin, Belfield, Dublin 4, Ireland, and Wuhan National Laboratory for Optoelectronics, Huazhong University of Science and Technology, Wuhan 430074, China

C. Suzuki
National Institute for Fusion Science, 322-6 Oroshi-cho, Toki 509-5292, Japan

(Received 22 October 2017; published 4 December 2017)

It is well known that the lanthanide and actinide elements are formed by the filling of $4f$ and $5f$ subshells which occurs after the filling of $5d$ and $6d$ subshells, respectively, has begun. With increasing ionization one expects the energy levels to eventually regroup to their hydrogenic ordering, i.e., in terms of principal quantum number. In the lanthanides, the $4f$ electron binding energy overtakes that of $5p$ near the 6th or 7th ion stage and $5s$ near the 14th or 15th ion stage, leading to dramatic rearrangements of ground-state configurations. In this paper we report on the results of a study to explore the effects of increasing ionization on the ground-state configurations of actinide ions as a result of $5f$ and $6p$ or $6s$ level crossings. It is seen that the effects generally occur later and are more strongly influenced by spin-orbit splitting than in the lanthanides. The near degeneracies of $5f$ and $6l$ energies in these stages lead to configuration interaction (CI) amongst configurations with variable numbers of $5f$ and $6p$ electrons. The effects of CI on the level complexity are explored for ions along the Rn I sequence and are found to lead to the formation of "compound states" as predicted for the lanthanides. The extreme ultraviolet and soft x-ray spectra of medium and highly charged lanthanides are dominated by emission from unresolved transition arrays (UTAs) of the type $\Delta n = 0$, $4p^6 4d^{N+1} - 4p^5 4d^{N+2} + 4p^6 4d^N 4f$, which, in general, overlap in adjacent ion stages of a particular element. Here, the corresponding $\Delta n = 0$, $5p^6 5d^{N+1} - 5p^5 5d^{N+2} + 5p^6 5d^N 5f$ UTAs have been studied theoretically with the aid of Hartree-Fock with configuration interaction calculations. As well as predicting the wavelengths and spectral details of the anticipated features, the calculations show that the effects of configuration interaction are quite different for the two different families of $\Delta n = 0$ transitions and, once more, spin-orbit interactions play a major role.

DOI: 10.1103/PhysRevA.96.062501

I. INTRODUCTION

It is well known that the lanthanide and actinide series of elements are formed by successive filling of electronic $4f$ and $5f$ subshells, in the elements following lanthanum ($Z = 57$) and thorium ($Z = 90$), respectively, as a result of f wave function collapse [1]. For neutral atoms of the elements from Ag to La, the effective radial potential consists of an attractive Coulomb and a centrifugal repulsion $l(l+1)/2\mu r^2$ term, where l is the orbital angular momentum quantum number and μ is the reduced mass of the electron. The resulting potential is bimodal, with an inner well close to the nucleus, whose depth rapidly increases from $Z = 47$ (silver), where a shallow minimum first appears, to $Z = 58$ (cerium), where it first supports a bound $4f$ state leading to the formation of the lanthanides [1–3]. In the elements preceding La ($Z = 57$), this inner well is separated by the centrifugal barrier from a broad outer well with a minimum near the hydrogenic value of $16a_0$ and its effective principal quantum number has been predicted to change abruptly from a value of $n \approx 4$ in Cs to $n < 2$ in La to $n \approx 1$ in Ce, where a $4f$ electron first appears in the ground state [4]. With increasing nuclear charge or degree of ionization, the inner well deepens and the barrier decreases, resulting in a mixing of the inner- and outer-well states [5,6]. In this context, it should be noted that the ground configuration of Ce is $(\mathrm{Xe})6s^2 5d 4f$ and in the excited $(\mathrm{Xe})6s^2 4f^2$ configuration the $4f$ electrons behave essentially as eigenstates of the different potential wells or, more correctly, as superpositions of inner- and outer-well functions [7]. Consequently, term-dependent calculations are required to correctly describe the resulting level structure which, in turn, limits the accuracy of any intermediate coupling calculation as the various interaction parameters depend strongly on the choice of wave function.

In a similar fashion, in the elements preceding protactinium, Pa ($Z = 91$), the $5f$ wave function is an eigenstate of an outer well with a minimum at $25a_0$ while the inner well only supports bound $4f$ states. With increasing Z, the inner well deepens sufficiently that at $Z = 91$ the $5f$ wave function is predicted to be essentially an eigenstate of the inner well and the lowest configuration is $(\mathrm{Rn})7s^2 6d 5f^2$ [4]. Also, with increasing Z, the $5f$ subshell gradually fills to form the actinide group of elements. Because of the more diffuse nature of the $5f$ wave function, the ground configurations of the lanthanides and their corresponding homologous actinides are not always necessarily the same, so simply changing the value of n to $n+1$ will not always define the lowest configuration. Already,

*john.sheil@ucdconnect.ie

TABLE I. Ground-state configurations of charge states I–XIII as tabulated in the NIST database [19]. For charge states I–XIII, ground-state configurations listed $5f^n$ have a Rn-like core, i.e., (Rn)$5f^n$.

	I	II	III	IV	V	VI	VII	VIII	IX	X	XI	XII	XIII
Ac	$6d7s^2$	$7s^2$	$7s$	$6p^6$	$6p^5$	$6p^4$	$6p^3$	$6p^2$	$6p$	$6s^2$	$6s$	$5d^{10}$	$5d^9$
Th	$6d^27s^2$	$6d7s^2$	$5f6d$	$5f$	$6p^6$	$6p^5$	$6p^4$	$6p^3$	$6p^2$	$6p$	$6s^2$	$6s$	$5d^{10}$
Pa	$5f^26d7s^2$	$5f^27s^2$	$5f^26d$	$5f^2$	$5f$	$6p^6$	$6p^5$	$6p^4$	$6p^3$	$6p^2$	$6p$	$6s^2$	$6s$
U	$5f^36d7s^2$	$5f^37s^2$	$5f^4$	$5f^3$	$5f^2$	$5f$	$6p^6$	$6p^5$	$6p^4$	$6p^3$	$6p^2$	$6p$	$6s^2$
Np	$5f^46d7s^2$	$5f^46d7s$	$5f^5$	$5f^4$	$5f^3$	$5f^2$	$5f$	$6p^55f$	$6p^45f$	$6p^35f$	$6p^25f$	$6p^2$	$6p$
Pu	$5f^67s^2$	$5f^67s$	$5f^6$	$5f^5$	$5f^4$	$5f^3$	$6p^55f^3$	$6p^45f^3$	$6p^35f^3$	$6p^25f^3$	$6p^25f^2$	$6p^25f$	$6p^2$
Am	$5f^77s^2$	$5f^77s$	$5f^7$	$5f^6$	$5f^5$	$5f^4$	$5f^3$	$6p^55f^3$	$6p^45f^3$	$6p^35f^3$	$6p^25f^3$	$6p^25f^2$	$6p^25f$
Cm	$5f^76d7s^2$	$5f^77s^2$	$5f^8$	$5f^7$	$5f^6$	$5f^5$	$5f^4$	$6p^45f^5$	$6p^35f^5$	$6p^25f^5$	$6p^25f^4$	$6p^25f^3$	$6p^25f^2$
Bk	$5f^97s^2$	$5f^97s$	$5f^9$	$5f^8$	$5f^7$	$5f^6$	$5f^5$	$5f^4$	$6p^35f^6$	$6p^25f^6$	$6p^25f^5$	$6p^25f^4$	$6p^25f^3$
Cf	$5f^{10}7s^2$	$5f^{10}7s$	$5f^{10}$	$5f^9$	$5f^8$	$5f^7$	$5f^6$	$5f^5$	$5f^4$	$6p^25f^7$	$6p^25f^6$	$6p^25f^5$	$6p^25f^4$
Es	$5f^{11}7s^2$	$5f^{11}7s$	$5f^{11}$	$5f^{10}$	$5f^9$	$5f^8$	$5f^7$	$5f^6$	$5f^5$	$5f^4$	$6p^25f^7$	$6p^25f^6$	$6p^25f^5$
Fm	$5f^{12}7s^2$	$5f^{12}7s$	$5f^{12}$	$5f^{11}$	$5f^{10}$	$5f^9$	$5f^8$	$5f^7$	$5f^6$	$5f^5$	$5f^4$	$6p^25f^7$	$6p^25f^6$
Md	$5f^{13}7s^2$	$5f^{13}7s$	$5f^{13}$	$5f^{12}$	$5f^{11}$	$5f^{10}$	$5f^9$	$5f^8$	$5f^7$	$5f^6$	$5f^5$	$5f^4$	$6p^25f^7$
No	$5f^{14}7s^2$	$5f^{14}7s$	$5f^{14}$	$5f^{13}$	$5f^{12}$	$5f^{11}$	$5f^{10}$	$5f^9$	$5f^8$	$5f^7$	$5f^6$	$5f^5$	$5f^4$
Lr	$5f^{14}7s^27p$	$5f^{14}7s^2$	$5f^{14}7s$	$5f^{14}$	$5f^{13}$	$5f^{12}$	$5f^{11}$	$5f^{10}$	$5f^9$	$5f^8$	$5f^7$	$5f^6$	$5f^5$

as we have seen, a $4f$ electron is present in the ground configuration of Ce, while the lowest configuration in the homologous species, Th, is (Rn)$7s^26d^2$ [8]. However, with increasing ionization the differences are predicted to diminish and by the 3rd ion stage the ground configurations of both sets of elements are expected to be of the same form, i.e., (Xe)$4f^n$ and (Rn)$5f^n$.

The primary purpose of the present paper is to explore how the correspondence of the lowest configurations between homologous actinide and lanthanide ions progresses as we proceed to higher ion stages. In the lanthanides, because of the tendency for electron energies to regroup according to their hydrogenic ordering, i.e., in terms of principal quantum number, with increasing ionization, the $4f$ binding energy increases more rapidly than that of either $5p$ or $5s$ as the $4f$ wave function contracts. A study based on the average energy of configuration ($E_{\rm av}$) calculations performed with Cowan's code [9] showed that $4f$ first crosses $5p$ near the 7th ion stage in elements up to and including $Z = 68$ and in the 8th ion stage of elements from $68 < Z < 71$ [10]. Thereafter, the lowest configurations contain a mixture of open $5p$ and $4f$ subshells until the 10th ion stage up to $Z = 66$ (Tb) and the 11th ion stage in elements with $Z > 66$. Subsequently the $4f$ and $5s$ levels cross at the 14th or 15th ion stage. As a result of these level crossings, complex configurations with variable numbers of $5p$ and $4f$ electrons overlap, frequently within a narrow energy range leading to significant configuration mixing and the formation of so-called "compound" or "chaotic" states. These states have properties exactly analogous to nuclear compound states observed as narrow resonances in low-energy neutron scattering whose adjacent level distributions follow a Wigner distribution [11–14]. For example, in Xe-like Sm IX, the lowest configuration is predicted to be $5p^34f^3$ and in ascending energy we have $5p^44f^2$, $5p^24f^4$, $5p4f^5$, $4f^6$, and $5p^6$, all of which lie within 20 eV or so of the ground state [15].

An early study to establish theoretical values of ionization potentials that included both highly charged lanthanides and actinides and was sensitive to level rearrangement predicted both $4f-5p$ and $4f-5s$ crossing to occur at ion stages lower than those established experimentally in the lanthanides [16]. These calculations included spin-orbit interaction and so introduced a large spin-orbit splitting that gave rise to mixed $4f$ and $5p$ configurations in a number of ion stages. Since jj-coupling is expected to be even more significant for the actinides, the combined effect of the diffuseness of the $5f$ wave function and the energy spread of the spin-orbit split $6p$ configuration was that the $5f-6p$ crossing was predicted to take place at higher ion stages and persist for longer than $4f-5p$ crossings in the lanthanides. In addition, the $5f-6s$ crossing was predicted not to be an issue in highly charged actinides [16]. Subsequently another set of calculations for ionization potentials were reported based on the fully relativistic Dirac-Fock approximation but to a large extent these ignored the effects of $5f$ contraction [17]. Ground-state configurations from the NIST database based on these works and the calculations of Cao and Dolg [18] are presented in Tables I and II [16–19]. An earlier study for all ion stages of U also did not show any evidence of $5f-6p$ level crossings in stages up to U^{11+}, where the $6p$ subshell empties, nor of $5f-6s$ crossings in the next two stages [20]. Much theoretical effort has, in fact, been directed towards the calculation of ionization potentials of U ions using increasingly refined theoretical approaches [21,22].

As might be expected, because of the highly transient nature and lack of availability of samples for spectroscopic analysis, experimental data for the majority of actinides in ion stages relevant to the present work are essentially nonexistent [8]. Very few experimental data exist to provide verification of the ground configurations of actinide ions. Whilst the ground configurations of many of the actinides have been established experimentally by spectroscopic studies, little work has been done on spectroscopy of their ions with the exception of the first few ions along the Fr-like [23,24] and Rn-like sequences [25]. The most detailed calculations on level structure and transition rates performed using relativistic many-body perturbation theory including the Breit interaction [26] and the relativistic intermediate Hamiltonian Fock-space coupled-cluster method, respectively

TABLE II. Ground-state configurations of charge states XIV–XXVI as tabulated in the NIST database [19]. For charge states XIV, ground-state configurations listed as $5f^n$ have a Rn-like core, i.e., (Rn)$5f^n$.

	XIV	XV	XVI	XVII	XVIII	XIX	XX	XXI	XXII	XXIII	XXIV	XXV	XXVI
Ac	$5d^8$	$5d^7$	$5d^6$	$5d^5$	$5d^4$	$5d^3$	$5d^2$	$5d$	$5p^6$	$5p^5$	$5p^4$	$5p^3$	$5p^2$
Th	$5d^9$	$5d^8$	$5d^7$	$5d^6$	$5d^5$	$5d^4$	$5d^3$	$5d^2$	$5d$	$5p^6$	$5p^5$	$5p^4$	$5p^3$
Pa	$5d^{10}$	$5d^9$	$5d^8$	$5d^7$	$5d^6$	$5d^5$	$5d^4$	$5d^3$	$5d^2$	$5d$	$5p^6$	$5p^5$	$5p^4$
U	$6s$	$5d^{10}$	$5d^9$	$5d^8$	$5d^7$	$5d^6$	$5d^5$	$5d^4$	$5d^3$	$5d^2$	$5d$	$5p^6$	$5p^5$
Np	$6s^2$	$6s$	$5d^{10}$	$5d^9$	$5d^8$	$5d^7$	$5d^6$	$5d^5$	$5d^4$	$5d^3$	$5d^2$	$5d$	$5p^6$
Pu	$6p$	$6s^2$	$6s$	$5d^{10}$	$5d^9$	$5d^8$	$5d^7$	$5d^6$	$5d^5$	$5d^4$	$5d^3$	$5d^2$	$5d$
Am	$6p^2$	$6p$	$6s^2$	$6s$	$5d^{10}$	$5d^9$	$5d^8$	$5d^7$	$5d^6$	$5d^5$	$5d^4$	$5d^3$	$5d^2$
Cm	$6p^25f$	$6p5f$	$5f$	$6s^2$	$6s$	$5d^{10}$	$5d^9$	$5d^8$	$5d^7$	$5d^6$	$5d^5$	$5d^4$	$5d^3$
Bk	$6p^25f^2$	$6p5f^2$	$5f^2$	$5f$	$6s^2$	$6s$	$5d^{10}$	$5d^9$	$5d^8$	$5d^7$	$5d^6$	$5d^5$	$5d^4$
Cf	$6p^25f^3$	$6p5f^3$	$5f^3$	$5f^2$	$5f$	$6s^2$	$6s$	$5d^{10}$	$5d^9$	$5d^8$	$5d^7$	$5d^6$	$5d^5$
Es	$6p^25f^4$	$6p5f^4$	$5f^4$	$5f^3$	$5f^2$	$5f$	$6s^2$	$6s$	$5d^{10}$	$5d^9$	$5d^8$	$5d^7$	$5d^6$
Fm	$6p^25f^5$	$6p5f^5$	$5f^5$	$5f^4$	$5f^3$	$5f^2$	$5f$	$6s^2$	$6s$	$5d^{10}$	$5d^9$	$5d^8$	$5d^7$
Md	$6p^25f^6$	$6p5f^6$	$5f^6$	$5f^5$	$5f^4$	$5f^3$	$5f^2$	$5f$	$6s^2$	$6s$	$5d^{10}$	$5d^9$	$5d^8$
No	$6p^25f^7$	$6p5f^7$	$5f^7$	$5f^6$	$5f^5$	$5f^4$	$5f^3$	$5f^2$	$5f$	$6s^2$	$6s$	$5d^{10}$	$5d^9$
Lr	$5f^4$	$6p5f^8$	$5f^8$	$5f^7$	$5f^6$	$5f^5$	$5f^4$	$5f^3$	$5f^2$	$5f$	$6s5f$	$5f$	$5d^{10}$

[27], have also concentrated on the lower ion stages of these two isoelectronic sequences. Also, the identification of some simple transitions of the type $5d^{10}6s^2-5d^96s^25f$ and $5d^{10}-5d^95f$ in the spectra of Th XI and Th XIII and U XIII and U XV [28,29] and the observation of broad, intense, unresolved transition arrays (UTAs) in extreme ultraviolet (EUV) spectra of laser-produced plasmas of these elements [30] and following uranium impurity injection in tokamak plasmas [31] have been reported. These UTAs were identified as arising from $5p^65d^{N+1}-5p^55d^{N+2}+5p^65d^N5f$ transitions and completely dominate the EUV emission in these plasmas. In the present work, calculations based on both Cowan's code [9] and the Flexible Atomic Code (FAC) [32] were performed to establish the ground configurations of actinide ions in stages where $5f-6p$ and $5f-6s$ level crossings can lead to electron rearrangement and, in addition, the predicted positions of $5p^65d^{N+1}-5p^55d^{N+2}+5p^65d^N5f$ UTAs are determined and their behavior is compared with the corresponding $n=4$-4 UTAs in the lanthanides. The high intensity of $4p^64d^{N+1}-4p^54d^{N+2}+4p^64d^N4f$ transitions has led to the development of plasma sources for applications of major technological importance ranging from lithography to biological imaging [33–35].

II. GROUND-STATE CONFIGURATIONS IN ACTINIDE IONS

Calculations were performed using the Hartree-Fock with Configuration Interaction (HFCI) suite of codes written by Cowan [9] to obtain $E_{\rm av}$ values. Because of the high Z of the atoms and ions of interest, relativistic effects, namely the mass-velocity and Darwin corrections were included. The Slater-Condon F^k, G^k, and R^k parameters were scaled to 85% of their *ab initio* values while the spin-orbit parameters were unchanged. Calculations were performed for ion stages from Au-like to Bk-like. Along the Au-, Hg-, Tl-, Pb-, and Bi-like isoelectronic sequences, calculations were performed for configurations with variable numbers of $5f$, $6s$, and $6p$ electrons. Thus, for example, in the particular case of the Bi I sequence, where the lowest configuration is expected to change from $6s^26p^3$ to $6s^25f^3$ and eventually to $5f^5$, all 15 configurations of the type $6s^M6p^K5f^N$ $(M+K+N=5)$ were included, i.e., $6s^26p^3$, $6s^26p^25f$, $6s^26p5f^3$, $6s6p^4$, $6s6p^35f$, $6s6p^25f^2$, $6s6p5f^3$, $6s5f^4$, $6p^5$, $6p^45f$, $6p^35f^2$, $6p^25f^3$, $6p5f^4$, and $5f^5$. Due to computational limitations, it was not possible to perform calculations with variable $5f/6s/6p$ occupancy for values of $M+K+N>5$. To this end, calculations for heavier sequences were performed with a closed $6s$ subshell. Although not as extensive a model as was adopted for the lighter isoelectronic sequences, one would expect, however, that the most important interactions for these heavier sequences would take place among configurations with variable $5f/6p$ occupancy. For each ion stage of each element, the configuration with the lowest average energy was taken to specify the ground configuration and the results are presented in Table III. From this table it is clearly seen that the $6p-5f$ crossing takes place at ion stages significantly higher than those in the corresponding lanthanides beginning at Pu^{13+}, then Am^{12+}, Cm^{11+}, Bk^{11+}, and Cf^{11+}, and then changing to the 10th ion stage in the heavier actinides. Also the $6s-5f$ level crossing is delayed so much that it does not impact the ground configuration of any of these ions.

However, the HFCI calculations also show that, as expected, spin-orbit splittings are larger for the actinides than for the lanthanides and the level structure is best defined by jj rather than LS coupling. In Fig. 1, the natural logarithm of the ratio of the Slater $F^2(nlnl)$ direct Coulomb interaction parameter to the spin-orbit parameter, ζ_{nl}, for $nl=5p$ and $4f$ along the Xe-like isoelectronic sequence for the configuration $5p^44f^2$ and for $nl=6p$ and $5f$ along the Rn-like isoelectronic sequence for the configuration $6p^45f^2$ are shown. It is clear from this figure that jj coupling increases in going from the lanthanides to the actinides and also provides the best description for the p electrons, while the reverse is true for the f electrons. Because the $6p$ spin-orbit splitting is much greater than the $5f$ spin-orbit splitting, the configuration with the lowest $E_{\rm av}$ may not necessarily correspond to that containing the lowest level. To explore this aspect, *ab initio* calculations

TABLE III. Ground-state configurations of numerous actinide ions calculated using Cowan's suite of codes. Discrepancies between the NIST database and the current set of calculations are highlighted in bold. All calculated ground-state configurations of charge states in the range XVII–XXIII are in full agreement with the NIST database. For charge states VII–XI, ground-state configurations listed as $5f^n$ have a Rn-like core, i.e., (Rn)$5f^n$.

	VII	VIII	IX	X	XI	XII	XIII	XIV	XV	XVI	...	XXIV	XXV
Ac	$6p^3$	$6p^2$	$6p$	$6s^2$	$6s$	$5d^{10}$	$5d^9$	$5d^8$	$5d^7$	$5d^6$		$5p^4$	$5p^3$
Th	$6p^4$	$6p^3$	$6p^2$	$6p$	$6s^2$	$6s$	$5d^{10}$	$5d^9$	$5d^8$	$5d^7$		$5p^5$	$5p^4$
Pa	$6p^5$	$6p^4$	$6p^3$	$6p^2$	$6p$	$6s^2$	$6s$	$5d^{10}$	$5d^9$	$5d^8$		$5p^6$	$5p^5$
U	$6p^6$	$6p^5$	$6p^4$	$6p^3$	$6p^2$	$6p$	$6s^2$	$6s$	$5d^{10}$	$5d^9$		$5d$	$5p^6$
Np	$5f$	**$6p^6$**	**$6p^5$**	**$6p^4$**	**$6p^3$**	$6p^2$	$6p$	$6s^2$	$6s$	$5d^{10}$		$5d^2$	$5d$
Pu	**$5f^2$**	**5f**	**$6p^6$**	**$6p^5$**	**$6p^4$**	**$6p^3$**	$6p^2$	**5f**	$6s^2$	$6s$		$5d^3$	$5d^2$
Am	$5f^3$	**$5f^2$**	**5f**	**$6p^6$**	**$6p^5$**	**$6p^4$**	$6p^2 5f$	**$5f^2$**	**5f**	$6s^2$		$5d^4$	$5d^3$
Cm	$5f^4$	**$5f^3$**	**$5f^2$**	**5f**	**$6p^6$**	**$6p^4 5f$**	$6p^2 5f^2$	**$5f^3$**	**$5f^2$**	$5f$		$5d^5$	$5d^4$
Bk	$5f^5$	$5f^4$	**$5f^3$**	**$5f^2$**	**5f**	**$6p^4 5f^2$**	$6p^2 5f^3$	**$5f^4$**	**$5f^3$**	$5f^2$		$5d^6$	$5d^5$
Cf	$5f^6$	$5f^5$	$5f^4$	**$5f^3$**	**$5f^2$**	**$6p^4 5f^3$**	**$6p5f^5$**	**$5f^5$**	**$5f^4$**	$5f^3$		$5d^7$	$5d^6$
Es	$5f^7$	$5f^6$	$5f^5$	$5f^4$	**$6p^5 5f^4$**	**$6p^3 5f^5$**	**$6p5f^6$**	**$5f^6$**	**$5f^5$**	$5f^4$		$5d^8$	$5d^7$
Fm	$5f^8$	$5f^7$	$5f^6$	$5f^5$	**$6p^5 5f^5$**	**$6p^3 5f^6$**	**$6p5f^7$**	**$5f^7$**	**$5f^6$**	$5f^5$		$5d^9$	$5d^8$
Md	$5f^9$	$5f^8$	$5f^7$	$5f^6$	**$6p^5 5f^6$**	**$6p^3 5f^7$**	**$5f^9$**	**$5f^8$**	**$5f^7$**	$5f^6$		$5d^{10}$	$5d^9$
No	$5f^{10}$	$5f^9$	$5f^8$	$5f^7$	**$6p^5 5f^7$**	**$6p^2 5f^9$**	**$5f^{10}$**	**$5f^9$**	**$5f^8$**	$5f^7$		$6s$	$5d^{10}$
Lr	$5f^{11}$	$5f^{10}$	$5f^9$	$5f^8$	**$6p^4 5f^9$**	**$6p^2 5f^{10}$**	**$5f^{11}$**	**$5f^{10}$**	**$5f^9$**	$5f^8$		**$6s^2$**	**6s**

were performed with the fully relativistic FAC which uses the Dirac equation as its starting point [32]. For ion stages in the range Au-like to Rn-like, calculations were performed with variable numbers of $5f/6s/6p$ occupancy, i.e. the same configuration basis as was used for the first set of Cowan's code calculations. Only configurations with variable $5f/6p$ occupancy were considered in the level-structure calculations for heavier isoelectronic sequences in the range Fr-like to Bk-like. Typically, in the FAC calculations, one optimizes the local central potential using a fictitious mean configuration with fractional occupation numbers. As advised by Gu [32] in the documentation accompanying the FAC package, it is best practice to construct this mean configuration from the lowest-lying configurations. However, in the presence of strong configuration mixing, it is quite difficult to determine an optimum mean configuration from which to derive the local central potential. To investigate this further, we performed two independent sets of calculations for each ion stage where we adopted as the mean configuration (i) the configuration belonging to the lowest-lying level, e.g., $6p^3 5f^3$, and (ii) the configuration associated with the next-lowest-lying level not belonging to the ground-state configuration, e.g., $6p^4 5f^2$. Clearly, the definition of a configuration in this context is quite ambiguous. The purpose of these calculations was to investigate the variation in calculated level energies using different mean configurations. For the vast majority of ion stages considered in this work, only slight variations in excited level energies were observed between calculations (i) and (ii) described above. Most importantly, both calculations consistently yielded the same ground-state configurations. The lowest configurations, based on the leading eigenvectors of the lowest energy levels, are presented in Table IV. Note that there are differences especially around the ground configurations for the 9th, 10th, and 14th to 16th ion stages with the NIST database. Compared to the results of the $E_{\rm av}$ calculation, some differences emerge, most notably the onset of level crossing begins at slightly lower ionization states such as Pu^{11+}, then Am^{9+}, and occurs at the 9th ionization stage for all of the heavier actinides with the exception of Es^{8+}. The $5f-6p$ crossing is predicted not to be fully completed until the 17th or 18th ion stage, while the $E_{\rm av}$ crossing is predicted by the HFCI calculations to happen before the 13th ion stage. As highlighted in Table IV, it was not possible to calculate the ground-state configuration of U VIII [NIST ground-state configuration: (Hg)$6p^5$]. The same was also true for Lr XXV [NIST ground-state configuration: (Xe)$4f^{14}5d^{10}5f$]. In both cases, a convergence issue was encountered in one of the FAC subroutines. Unfortunately, an effort to increase the maximum number of iterations to allow for convergence proved futile. Finally, it is interesting to note that the lowest configuration in no ion in this table contains a $5f$ electron rather than a $6s$ electron.

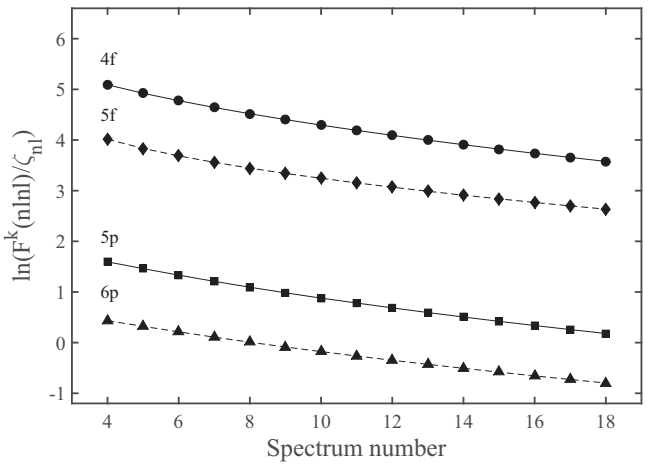

FIG. 1. Logarithmic dependence of the ratio $F^k(nlnl)/\zeta_{nl}$ on the spectrum number. Data points connected by dashed lines correspond to actinide ions, with diamonds and triangles representing $nl = 5f$ and $6p$, respectively. Data points connected by unbroken lines correspond to lanthanide ions, with circles and squares representing $nl = 4f$ and $5p$, respectively.

TABLE IV. Ground-state configurations of numerous actinide ions calculated using the FAC. Discrepancies between the NIST database and the current calculations are highlighted in bold. All calculated ground-state configurations of charge states in the range XIX–XXIII are in full agreement with the NIST database. For charge states VII–IX, ground-state configurations listed as $5f^n$ have a Rn-like core, i.e., (Rn)$5f^n$. *Calculation did not converge—corresponding NIST entry tabulated.

	VII	VIII	IX	X	XI	XII	XIII	XIV	XV	XVI	XVII	XVIII	...	XXIV
Ac	$6p^3$	$6p^2$	$6p$	$6s^2$	$6s$	$5d^{10}$	$5d^9$	$5d^8$	$5d^7$	$5d^6$	$5d^5$	$5d^4$		$5p^4$
Th	$6p^4$	$6p^3$	$6p^2$	$6p$	$6s^2$	$6s$	$5d^{10}$	$5d^9$	$5d^8$	$5d^7$	$5d^6$	$5d^5$		$5p^5$
Pa	$6p^5$	$6p^4$	$6p^3$	$6p^2$	$6p$	$6s^2$	$6s$	$5d^{10}$	$5d^9$	$5d^8$	$5d^7$	$5d^6$		$5p^6$
U	$6p^6$	$6p^{5*}$	$6p^4$	$6p^3$	$6p^2$	$6p$	$6s^2$	$6s$	$5d^{10}$	$5d^9$	$5d^8$	$5d^7$		$5d$
Np	$5f$	$\mathbf{6p^6}$	$\mathbf{6p^5}$	$\mathbf{6p^4}$	$\mathbf{6p^3}$	$6p^2$	$6p$	$6s^2$	$6s$	$5d^{10}$	$5d^9$	$5d^8$		$5d^2$
Pu	$\mathbf{5f^2}$	$\mathbf{5f}$	$\mathbf{6p^6}$	$\mathbf{6p^5}$	$\mathbf{6p^4}$	$6p^25f$	$6p^2$	$6p$	$6s^2$	$6s$	$5d^{10}$	$5d^9$		$5d^3$
Am	$5f^3$	$\mathbf{5f^2}$	$\mathbf{5f}$	$\mathbf{6p^55f}$	$\mathbf{6p^45f}$	$6p^25f^2$	$6p^25f$	$6p^2$	$6p$	$6s^2$	$6s$	$5d^{10}$		$5d^4$
Cm	$5f^4$	$\mathbf{5f^3}$	$\mathbf{5f^2}$	$\mathbf{6p^55f^2}$	$\mathbf{6p^35f^3}$	$6p^25f^3$	$6p^25f^2$	$6p^25f$	$\mathbf{6p^2}$	$\mathbf{6p}$	$6s^2$	$6s$		$5d^5$
Bk	$5f^5$	$5f^4$	$\mathbf{5f^3}$	$\mathbf{6p^45f^4}$	$\mathbf{6p^35f^4}$	$6p^25f^4$	$6p^25f^3$	$6p^25f^2$	$\mathbf{6p^25f}$	$\mathbf{6p^2}$	$\mathbf{6p}$	$6s^2$		$5d^6$
Cf	$5f^6$	$5f^5$	$5f^4$	$\mathbf{6p^45f^5}$	$\mathbf{6p^35f^5}$	$6p^25f^5$	$6p^25f^4$	$6p^25f^3$	$\mathbf{6p^25f^2}$	$\mathbf{6p^25f}$	$\mathbf{6p^2}$	$5f$		$5d^7$
Es	$5f^7$	$5f^6$	$\mathbf{6p^55f^6}$	$\mathbf{6p^45f^6}$	$\mathbf{6p^35f^6}$	$6p^25f^6$	$6p^25f^5$	$6p^25f^4$	$\mathbf{6p^25f^3}$	$\mathbf{6p^25f^2}$	$\mathbf{6p^25f}$	$5f^2$		$5d^8$
Fm	$5f^8$	$5f^7$	$5f^6$	$\mathbf{6p^45f^7}$	$\mathbf{6p^35f^7}$	$6p^25f^7$	$6p^25f^6$	$6p^25f^5$	$\mathbf{6p^25f^4}$	$\mathbf{6p^25f^3}$	$\mathbf{6p5f^3}$	$5f^3$		$5d^9$
Md	$5f^9$	$5f^8$	$5f^7$	$\mathbf{6p^55f^7}$	$\mathbf{6p^45f^7}$	$\mathbf{6p^25f^8}$	$6p^25f^7$	$6p^25f^6$	$\mathbf{6p^25f^5}$	$\mathbf{6p^25f^4}$	$\mathbf{6p^25f^3}$	$\mathbf{6p5f^3}$		$5d^{10}$
No	$5f^{10}$	$5f^9$	$5f^8$	$\mathbf{6p^45f^9}$	$\mathbf{6p^35f^9}$	$\mathbf{6p^25f^9}$	$\mathbf{6p^25f^8}$	$6p^25f^7$	$\mathbf{6p^25f^6}$	$\mathbf{6p^25f^5}$	$\mathbf{6p^25f^4}$	$\mathbf{6p5f^4}$		$6s$
Lr	$5f^{11}$	$5f^{10}$	$5f^9$	$\mathbf{6p^45f^{10}}$	$\mathbf{6p^35f^{10}}$	$\mathbf{6p^25f^{10}}$	$\mathbf{6p^25f^9}$	$\mathbf{6p^25f^8}$	$\mathbf{6p^25f^7}$	$\mathbf{6p^25f^6}$	$\mathbf{6p^25f^5}$	$\mathbf{6p5f^5}$		$\mathbf{6s^2}$

In order to estimate where the $5f$ and $6s$ levels would cross in heavier elements, calculations were performed using the FAC for ions of the Rn-like isoelectronic sequence. Calculations were performed for all possible $6s^M6p^K5f^N$ $(M+K+N=8)$ configurations. The change in positions of the lowest levels of the $6s^26p^6$, $6s^26p^55f$, $6s^26p^45f^2$, $6s^26p^35f^3$, $6s^26p^25f^4$, $6s^26p5f^5$, $6s^25f^6$, $6s5f^7$, and $5f^8$ configurations with increasing ionization are shown in Fig. 2, which clearly shows the gradual change from $6s^26p^6$ past Pu^{8+} to $6s^25f^6$ at Rf^{18+}. The inset shows a continuation of the calculation for the lowest levels of the $5f^8$, $6s5f^7$, and $6s^25f^6$ configurations (curves A, B, and C) up to $Z=109$. Unfortunately, the FAC did not run for elements past $Z=109$. Therefore, we carried out two separate least-squares fits for the data points between $Z=104$ and 109 and extrapolated these fits to a level energy of 0 eV. From the plot one can see that the $5f$ level first falls below the $6s$ level at $Z\approx121$ (36th ion stage), with $5f^8$ becoming the ground-state configuration at $Z\approx123$. This situation is in stark contrast with the analogous case in the lanthanides where one would expect to see a $5s-4f$ level crossing for the Xe-like sequence occurring around the 16th ion stage [10].

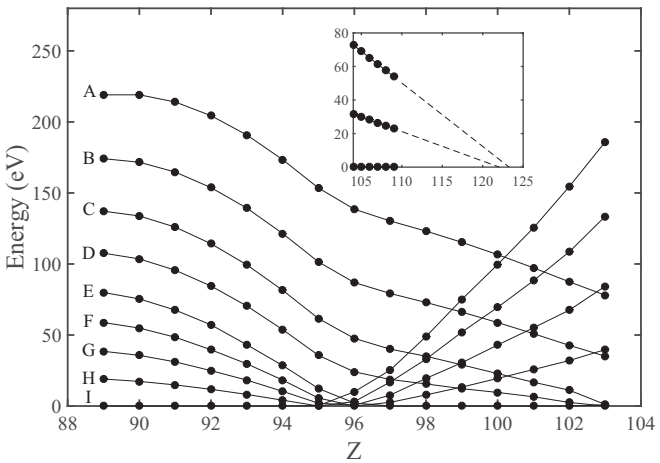

FIG. 2. Lowest-lying energy levels of numerous configurations along the Rn-like isoelectronic sequence. Curves A–I correspond to the configurations $5f^8$, $6s5f^7$, $6s^25f^6$, $6s^26p5f^5$, $6s^26p^25f^4$, $6s^26p^35f^3$, $6s^26p^45f^2$, $6s^26p^55f$, and $6s^26p^6$. The inset shows a continuation of curves A, B, and C up to $Z=109$, with a linear extrapolation being performed above $Z=109$.

III. STATISTICS OF $6s^M6p^K5f^N$ CONFIGURATIONS

According to the FAC calculations as shown in the preceding figure, the lowest configuration in Rn-like Cm^{10+} is $6s^26p^35f^3$, and the predicted level structure for the $6s^26p^K5f^N$ $(K+N=6)$ configurations is presented in Fig. 3. From this figure, it is clear that because many of these configurations overlap in energy there will be strong

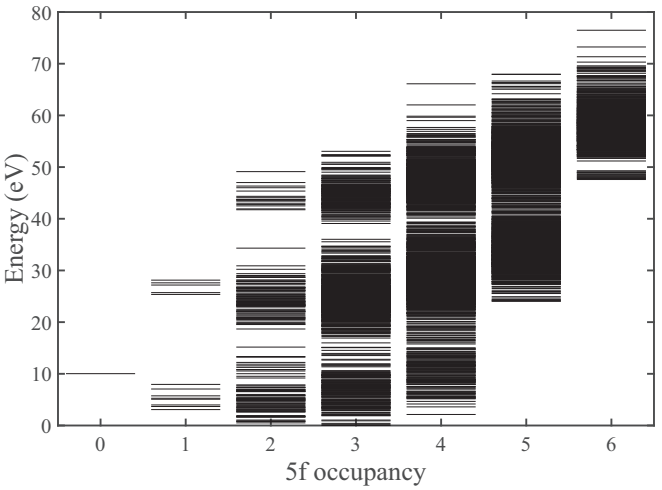

FIG. 3. Energies of levels belonging to Rn-like Cm^{10+}. Configurations with variable $5f/6p$ occupancy are shown.

configuration mixing. The FAC calculations include configuration interaction (CI) effects and the level assignments are based on leading eigenvector compositions. In the Xe-like isoelectronic sequence, the lowest configuration in Sm^{8+} was found to be $5s^2 5p^3 4f^3$, and because of CI effects, the nearest-neighbor separation of levels was found to follow a Wigner distribution, as mentioned earlier [15]. Flambaum and co-workers [36] showed that if the mean level spacing is D and the mean off-diagonal parameter is V, then the ratio V/D determines the level distribution. If V/D is large, there is a complete breakdown of the single-particle model and the resulting states are so highly mixed that only the total angular momentum J and the parity π are "good" quantum numbers. Moreover, the level density is such that the dynamical properties can be modeled using random matrix theory and obey Gaussian orthogonal ensemble statistics. This situation was shown to pertain to Sm^{8+} [37] and it was further shown that, as in earlier work [36], the off-diagonal elements tend to vanish between states well displaced in energy from any particular state in question, giving rise to the concept of a "spreading width" Γ, where $\Gamma = N_{\rm eig} D$ and $N_{\rm eig}$ is the number of eigenvector or single-particle basis-state components present in the mixed basis state in question. Thus if the states are arranged in order of ascending energy, the random matrices are "banded" or have finite off-diagonal elements arranged around the diagonal. Under these conditions, the nearest-neighbor separations in sets with the same J^π follow a Wigner distribution. The presence of a Wigner distribution of nearest-neighbor separations is a necessary but insufficient condition for the emergence of quantum chaos. For a Wigner distribution, the probability density function for a normalized nearest-neighbor spacing (NNS), s, is given by

$$P(s) = \frac{\pi s}{2} \exp\left(\frac{-\pi s^2}{4}\right). \quad (1)$$

Since compound states clearly result from level crossing and configuration interaction in lanthanide ions, it is reasonable to expect that they will also appear in actinide ions. However, as has been shown by numerous authors, the level statistics of atomic systems subject to strong configuration mixing are often best described as somewhere between the extremes of "regular" (Poisson) and "chaotic" (Wigner) behavior. This intermediate behavior can be described quantitatively using the Brody distribution [38,39], which is given by

$$P_q(s) = \alpha(q+1)s^q \exp(-\alpha s^{q+1}), \quad (2)$$

where $\alpha = [\Gamma(\frac{q+2}{q+1})]^{q+1}$ and q is known as the Brody or repulsion parameter. The Brody distribution reduces to the Poisson/Wigner distributions when $q = 0$ or 1, respectively. We evaluated the Brody parameter for the $J^\pi = 5^+$ interacting set in Rn-like Cm^{10+} using the T-function approach of Prozen and Robnik [40,41], described in detail by Cummings *et al.* [42] and Kilbane *et al.* [37]. We have obtained a value of $q = 0.932 \pm 0.017$ for the Brody parameter, indicating the existence of strong level repulsion in this spectrum. Details of this calculation will be described in a future comparative study of quantum chaotic signatures in lanthanide and actinide ions. In Fig. 4 the distribution of normalized NNSs for this interacting set are presented along with a Brody distribution having the Brody parameter $q = 0.932$. In a recent study, Viatkina *et al.* [43] have shown that levels belonging to independent J^π manifolds of the Pa atom exhibit signatures of a many-body quantum chaotic system. For example, they obtained a repulsion parameter of $q = 0.89 \pm 0.11$ for the $J^\pi = 7/2^+$ manifold of neutral Pa. Therefore, as in the case for the lanthanides, the level rearrangement results in the formation of compound states. The total energy spread of $6s^M 6p^K 5f^N$ $(M + K + N = 8)$ in Rn-like Cm^{10+} is ≈170 eV compared to ≈100 eV for $5s^M 5p^K 4f^N$ $(M + K + N = 8)$ in Sm^{8+}, whilst the corresponding numbers for $6s^2 6p^K 5f^N$ $(K + N = 6)$ and $5s^2 5p^K 4f^N$ $(K + N = 6)$ are ≈80 eV and ≈20 eV, respectively. The larger value of the former is due to the larger $6p$ splitting [ζ_{6p} (Cm^{10+}) = 12.52 eV, ζ_{5p} (Sm^{8+}) = 3.67 eV].

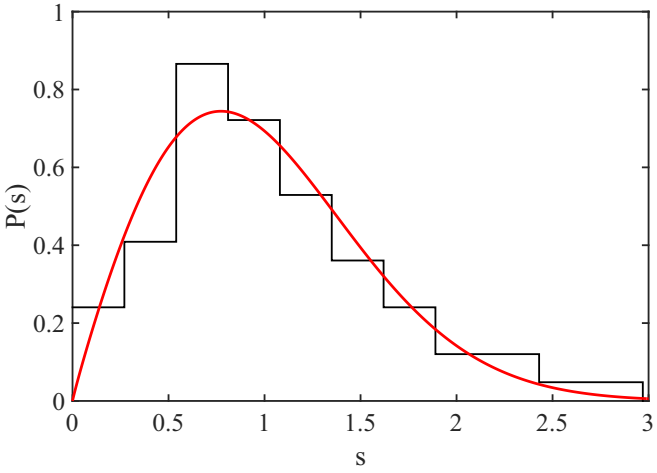

FIG. 4. NNS distribution for the $J^\pi = 5^+$ interacting set in Rn-like Cm^{10+}. The dimensionless spacings s are defined on the unfolded energy scale and the histogram is normalized to unity. A Brody distribution with the Brody parameter $q = 0.932$ is shown in red (curved line).

IV. 5*p*-5*d* and 5*d*-5*f* UNRESOLVED TRANSITION ARRAYS OF IONS WITH *Z* = 89-103

Energies were determined for $5p^6 5d^{N+1} - 5p^5 5d^{N+2} + 5p^6 5d^N 5f$ transitions both with and without CI for all ions with N = 0-8 of the elements considered. For the CI calculations, the eigenvector percentage compositions were used to assign $5d-5f$ and $5p-5d$ lines within the overall arrays. The results of these calculations are presented in Fig. 5 for ions of the elements Ac ($Z = 89$), Cm ($Z = 96$), and Lr ($Z = 103$). As noted in a recent study for n = 5-5 transitions in lower-Z elements, in the absence of CI the $5p-5d$ array splits due to spin-orbit interaction into $5p_{1/2}-5d$ and $5p_{3/2}-5d$ subarrays. The $5d-5f$ transition array is dominated by the $5d-5f$ electrostatic interaction due to the large overlap of the $5d$ and $5f$ wave functions and lies between the peak intensity regions of the $5p_{1/2}-5d$ and $5p_{3/2}-5d$ subarrays in every spectrum. The effect of CI is to modify the spectral profile and increase the overall intensity of the $5p_{1/2}-5d$ subarray while leaving its mean position essentially unchanged. The mixing of the $5d-5f$ and $5p_{3/2}-5d$ arrays also alters the spectral profiles and shifts the mean energy of the $5d-5f$ array to a

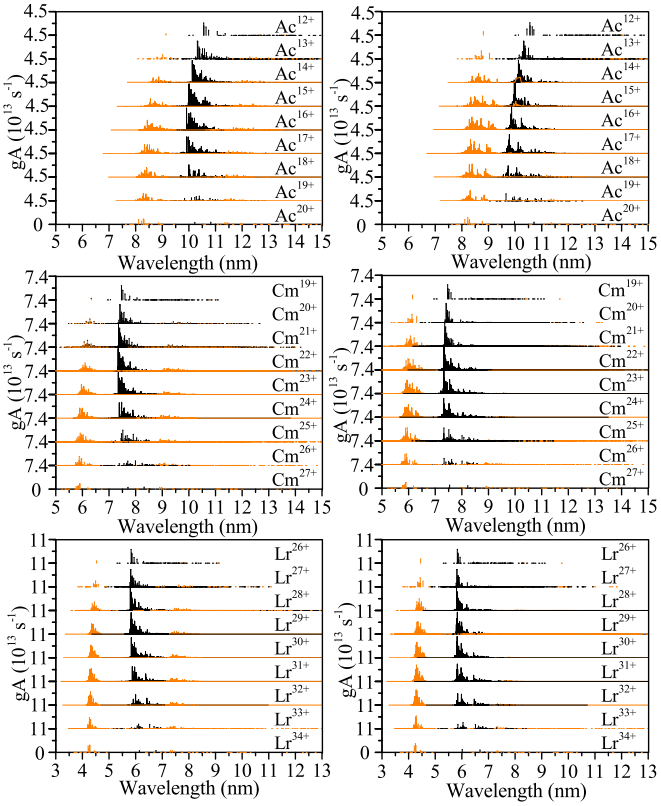

FIG. 5. Calculated positions of $\Delta n = 0$, $5p^6 5d^{N+1} - 5p^5 5d^{N+2} + 5p^6 5d^N 5f$ transitions for Ac, Cm, and Lr calculated using Cowan's suite of codes excluding CI (left) and including CI (right). Black denotes $5d-5f$ transitions and orange (gray) denotes $5p-5d$ transitions.

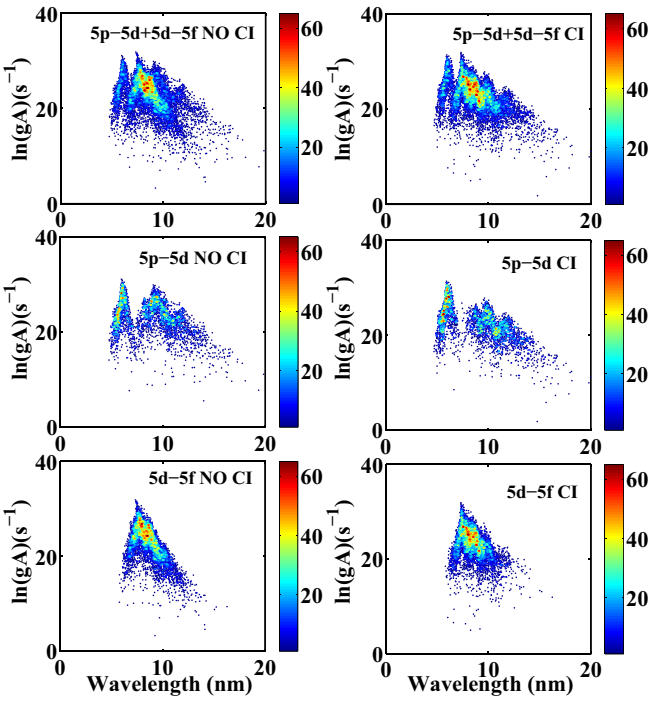

FIG. 6. Calculated gA values versus wavelength data for Cm^{23+} for $\Delta n = 0$, $5p^6 5d^5 - 5p^5 5d^6 + 5p^6 5d^4 5f$ transitions shown in the form of binned scatter plots, where the color bar corresponds to the relative density of transition points within the bins. Each bin was of size 0.1 nm × 0.1 s^{-1} [ln(gA)] for each scatter plot.

shorter wavelength while the $5p_{3/2}-5d$ array appears to be almost completely quenched and its intensity appears to be shared among the lower-energy arrays. To further illustrate this behavior, in Fig. 6, a scatter plot of calculated gA values versus wavelength data for the $5p^6 5d^5 - 5p^5 5d^6 + 5p^6 5d^4 5f$ transitions in Cm^{23+} is shown in the form of binned scatter plots, where the color bar corresponds to the relative density of transition points within the bins. Each bin was of size 0.1 nm × 0.1 s^{-1} [ln(gA)] for each scatter plot. It is clearly seen that the majority of the transitions are very weak. The total array width is close to 200 eV, with the $5p^6 5d^5 - 5p^5 5d^6$ subset essentially splitting into two subarrays, and there is considerable overlap with $5p^6 5d^5 - 5p^6 5d^4 5f$ transitions. The effect of CI is to decrease the intensities of the strongest lines in the longer-wavelength $5p^6 5d^5 - 5p^5 5d^6$ subarray, while at the same time causing some redistribution of oscillator strength amongst the $5d-5f$ transitions while the shorter-wavelength $5p-5d$ subarray remains essentially unchanged. Thus the effect of CI for 5-5 transitions is far less dramatic than that for the corresponding $4p^6 4d^{N+1} - 4p^5 4d^{N+2} + 4p^6 4d^N 4f$ transitions in lanthanide spectra where it leads to complex redistribution of oscillator strength to the higher-energy end of the array and causes a pronounced spectral narrowing [44–46]. In addition, in the lanthanides, the $4d-4f$ transition arrays in a particular element move to longer wavelength with increasing ionisation [10], while in the case of the $5d-5f$ arrays in actinides, apart from some shift towards a shorter wavelength at the beginning of the sequence, evident here in the Ac spectra, they remain at essentially the same wavelength with ascending ionization both with and without CI. In the absence of CI, according to the UTA formalism, for $4p^6 4d^{N+1} - 4p^5 4d^{N+2} + 4p^6 4d^N 4f$ transitions the position of the line strength weighted mean of an array is shifted from the position of the differences in average energies by the following amount [47]:

$$\delta E = \frac{35}{9}(N)\left(\sum_{k\neq 0} f_k F^k(4d4f) + \sum_k g_k G^k(4d4f)\right), \quad (3)$$

where $F^k(4d4f)$ and $G^k(4d4f)$ are Slater-Condon direct and exchange integrals, respectively, and the coefficients f_k and g_k result from integrals over polar and azimuthal angles that, in general, decrease with increasing k [48]. Here g_1 has the largest numerical value and the reduction in N is balanced by an increase in the value of the Slater-Condon parameters.

The shift towards a shorter wavelength at the lower-Z end of the sequence as seen in the Ac spectra in Fig. 5 arises due to $5f$ orbital contraction [49]. From a comparison with experimental spectra of highly ionized Th and U it was inferred that the calculated results for the $5d-5f$ transitions agree quite well with experimentally observed UTA positions [44]. Thus, as in the case of the lanthanides, where an intense UTA due to $4d-4f$ transitions is observed, $5d-5f$ transitions dominate the observed spectra of ion stages with an open $5d$ subshell [49]. The calculated positions of the $5p-5d$

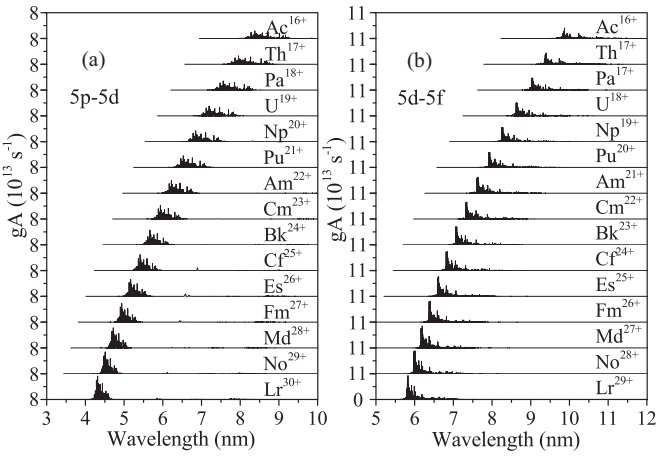

FIG. 7. Calculated positions of the $5p-5d$ and $5d-5f$ transition arrays in the actinides along the Re I isoelectronic sequence [ground-state configuration (Xe)$4f^{14}5p^{6}5d^{5}$].

and $5d-5f$ arrays along the Re I isoelectronic sequence [ground configuration (Xe)$4f^{14}5p^{6}5d^{5}$], identified from the upper-state leading eigenvectors, are shown in Fig. 7 and clearly show the progression to shorter wavelengths of both families of transitions with increasing Z. They also clearly show the quenching of the $5p_{3/2}-5d$ array.

V. CONCLUSION

We have shown that $5f-6p$ level crossing effects along different isoelectronic sequences lead to significant changes in ground-state configurations in actinide ions and that strong configuration interaction between configurations containing variable numbers of $6p$ and $5f$ electrons resulting from the near degeneracies of $5f$ and $6p$ binding energies leads to the formation of compound states and the complete breakdown of a single-particle picture in describing the level structure. In this regard there are strong similarities with the behavior associated with $4f-5p$ and $4f-5s$ level crossings in lanthanide ions, though there are differences for homologous ions. First, the greater influence of relativistic effects in the actinides means that the $6p$ configuration widths are significantly greater due to spin-orbit interaction, and in addition, $5f-6s$ level crossing does not cause any changes in ground configurations of the actinides. Since the dominant features in ionized rare-earth spectra are UTAs resulting from $\Delta n = 0, 4d-4f$ and $4p-4d$ transitions, we have also considered the corresponding $\Delta n = 0$, $5d-5f$ and $5p-5d$ transitions in the actinides. Once more, spin-orbit splitting was found to lead to significant differences between both sets of spectra. Finally, we hope that these results will stimulate further calculations to explore the effects of, for example, the Breit interaction on the level structure of the ions considered here.

ACKNOWLEDGMENTS

J.S. acknowledges funding from the Irish Research Council (GOIPG/2015/3756). L.L. acknowledges support from UCD and from a Chinese Scholarship Council scholarship [Fundamental Research Funds for the Central Universities (HUST:2016YXMS028)]. D.K. acknowledges funding from the Irish Research Council and a Marie Curie Actions ELEVATE fellowship (ELEVATEPD/2013/11).

[1] M. G. Mayer, Phys. Rev. **60**, 184 (1941).
[2] T. Y. Wu, Phys. Rev. **44**, 727 (1933).
[3] A. R. P. Rao and U. Fano, Phys. Rev. **167**, 7 (1968).
[4] D. C. Griffin, K. L. Andrews, and R. D. Cowan, Phys. Rev. **177**, 62 (1969).
[5] J. P. Connerade and M. W. D. Mansfield, Phys. Rev. Lett. **48**, 131 (1982).
[6] A. Cummings, C. McGuinness, G. O'Sullivan, J. T. Costello, J. P. Mosnier, and E. T. Kennedy, Phys. Rev. A **63**, 022702 (2001).
[7] S. Kučas and R. Karaziya, Phys. Scr. **58**, 220 (1998).
[8] J. Blaise and J. F. Wyart, *Energy Levels and Atomic Spectra of Actinides*, International Tables of Selected Constants (Tables Internationales de Constantes, Paris, 1992), No. 20.
[9] R. D. Cowan, *The Theory of Atomic Structure and Spectra* (University of California, Berkeley, 1981).
[10] D. Kilbane and G. O'Sullivan, Phys. Rev. A **82**, 062504 (2010).
[11] V. V. Flambaum, A. A. Gribakina, and G. F. Gribakin, Phys. Rev. A **58**, 230 (1998).
[12] A. A. Gribakina and G. F. Gribakin, J. Phys. B **29**, L809 (1996).
[13] V. Zelevinsky, B. A. Brown, N. Frazier, and M. Horoi, Phys. Rep. **276**, 85 (1996).
[14] G. O'Sullivan, P. K. Carroll, P. Dunne, R. Faulkner, C. McGuinness, and N. Murphy, J. Phys. B **32**, 1893 (1999).
[15] D. Kilbane, A. Cummings, C. McGuinness, N. Murphy, and G. O'Sullivan, J. Phys. B **35**, 309 (2002).
[16] T. A. Carlson, C. W. Nestor, N. Wasserman, and J. D. Mcdowell, At. Data Nucl. Data Tables **2**, 63 (1970).
[17] G. C. Rodrigues, P. Indelicato, J. P. Santos, P. Patte, and F. Parente, At. Data Nucl. Data Tables **86**, 117 (2004).
[18] X. Cao and M. Dolg, Mol. Phys. **101**, 961 (2003).
[19] A. Kramida, Yu. Ralchenko, J. Reader, and NIST ASD Team, NIST Atomic Spectra Database (ver. 5.3), available at http://physics.nist.gov/asd (2017, September 21), National Institute of Standards and Technology, Gaithersburg, MD, 2015.
[20] K. Rashid, M. Z. Saadi, and M. Yasin, At. Data Nucl. Data Tables **40**, 365 (1988).
[21] A. Weigand, X. Cao, T. Hangele, and M. Dolg, J. Phys. Chem. A **118**, 2519 (2014).
[22] D. H. Bross, P. Parmar, and K. A. Petersen, J. Chem. Phys. **143**, 184308 (2015).
[23] J. A. Keele, M. E. Hanni, S. L. Woods, S. R. Lundeen, and C. W. Fehrenbach, Phys. Rev. A **83**, 062501 (2011).
[24] M. E. Hanni, S. R. Lundeen, and C. W. Fehrenbach, Bull. Am. Phys. Soc. **55**, BAPS.2010.DAMOP.C5.7 (2010).
[25] J. A. Keele, S. R. Lundeen, and C. W. Fehrenbach, Phys. Rev. A **83**, 062509 (2011).
[26] U. I. Safronova and M. S. Safronova, Phys. Rev. A **84**, 052515 (2011).
[27] E. Eliav and U. Kaldor, Chem. Phys. **392**, 78 (2012).

[28] P. K. Carroll, J. Costello, E. T. Kennedy, and G. O'Sullivan, J. Phys. B **17**, 2169 (1984).
[29] P. K. Carroll, J. T. Costello, E. T. Kennedy, and G. O'Sullivan, J. Phys. B **19**, L651 (1986).
[30] P. K. Carroll and G. O'Sullivan, Phys. Lett. A **84**, 59 (1981).
[31] M. Finkenthal, S. Lippmann, H. W. Moos, P. Mandelbaum, and TEXT Group, Phys. Rev. A **39**, 3717(R) (1989).
[32] M. F. Gu, Can. J. Phys. **86**, 675 (2008).
[33] W. van der Zande, in *Proceedings of the 2016 International Workshop on EUV and Soft X-ray Sources, November 7–9, 2016, Amsterdam, The Netherlands*, edited by V. Bakshi (EUV Litho, Inc., Austin, Texas, 2016).
[34] G. O'Sullivan, B. W. Li, R. D'Arcy, P. Dunne, P. Hayden, D. Kilbane, T. McCormack, H. Ohashi, F. O'Reilly, P. Sheridan, E. Sokell, C. Suzuki, and T. Higashiguchi, J. Phys. B **48**, 144025 (2015).
[35] T. Higashiguchi, T. Otsuka, N. Yugami, W. Jiang, A. Endo, B. Li, P. Dunne, and G. O'Sullivan, Appl. Phys. Lett. **100**, 014103 (2012).
[36] V. V. Flambaum, A. A. Gribakina, G. F. Gribakin, and M. G. Kozlov, Phys. Rev. A **50**, 267 (1994).
[37] D. Kilbane, A. Cummings, D. M. Heffernan, and G. O'Sullivan, Phys. Scr. **73**, 198 (2006).
[38] T. A. Brody, J. Flores, J. B. French, P. A. Mello, A. Pandey, and S. S. M. Wong, Rev. Mod. Phys. **53**, 385 (1981).
[39] J. P. Connerade, I. P. Grant, P. Marketos, and J. Oberdisse, J. Phys. B **28**, 2539 (1995).
[40] T. Prozen and M. Robnik, J. Phys. A: Math Gen. **26**, 2371 (1993).
[41] K. Ganesan and M. Lakshmanan, J. Phys. B **27**, 2809 (1994).
[42] A. Cummings, G. O'Sullivan, and D. M. Heffernan, J. Phys. B **34**, 3447 (2001).
[43] A. V. Viatkina, M. G. Kozlov, and V. V. Flambaum, Phys. Rev. A **95**, 022503 (2017).
[44] P. Mandelbaum, M. Finkenthal, J. L. Schwob, and M. Klapisch, Phys. Rev. A **35**, 5051 (1987).
[45] J. Bauche, C. Bauche-Arnoult, M. Klapisch, P. Mandelbaum, and J. L. Schwob, J. Phys. B **20**, 1443 (1987).
[46] F. Koike, S. Fritzsche, K. Nishihara, A. Sasaki, T. Kagawa, T. Nishikawa, K. Fujima, T. Kawamura, and H. Furukawa, J. Plasma Fusion Res. SERIES **7**, 253 (2006).
[47] C. Bauche-Arnoult, J. Bauche, and M. Klapisch, Phys. Rev. A **20**, 2424 (1979).
[48] E. U. Condon and H. Odabasi, *Atomic Structure* (Cambridge University, Cambridge, England, 1980).
[49] L. Liu, D. Kilbane, P. Dunne, X. Wang, and G. O'Sullivan, Atoms **5**, 20 (2017).